Available online at www.sciencedirect.com
ScienceDirect
Trans. Nonferrous Met. Soc. China 33(2023) 3406−3417
Transactions of Nonferrous Metals Society of China
www.tnmsc.cn

Influences of Si and C addition on microstructure and mechanical properties of $Fe_{2.5}CoNiCu$ high-entropy alloy

Jian WU[1], Huan QIU[1], He-guo ZHU[1], Zong-han XIE[2], Jia-lin CHENG[3]

1. College of Materials Science and Engineering, Nanjing University of Science and Technology, Nanjing 210094, China;
2. School of Mechanical Engineering, University of Adelaide, SA 5005, Australia;
3. School of Materials of Science and Engineering, Nanjing Institute of Technology, Nanjing 210094, China

Received 29 April 2022; accepted 17 August 2022

Abstract: To evaluate the role of non-metallic element (Si and C) on the microstructural evolution and mechanical properties of $Fe_{2.5}CoNiCu$ high-entropy alloys (HEAs), two series of $Fe_{2.5}CoNiCuSi_x$ (x=0.1−0.3, molar fraction) and $Fe_{2.5}CoNiCuC_x$ (x=0.15−0.4, molar fraction) HEAs were prepared by vacuum induction melting. The results show that the amounts of C and Si additions significantly stimulate the transformation of BCC/FCC dual phases into a single FCC structure, and the microstructural evolution appears to be more strongly influenced by the C addition. The $Fe_{2.5}CoNiCuSi_{0.2}$ HEA presents high hardness (HV 439.5) and tensile strength (868 MPa), which is attributed to the solution strengthening and grain refinement effect. Both the hardness and strength of $Fe_{2.5}CoNiCuC_x$ HEAs increase with the addition of C, due to the formation of carbides and solution strengthening. This demonstrates that adding non-metallic element (C or Si) is a viable approach for enhancing the strength and hardness of HEAs.

Key words: high-entropy alloy; microstructural evolution; mechanical properties; non-metallic element addition; fracture mechanism

1 Introduction

High-entropy alloys (HEAs) have attracted much attention since they were first reported in 2004 [1]. HEAs are defined hence to compose of at least four or more principal elements with concentrations ranging from 5 to 35 at.%, which typically form a single-phase solid solution with face-centered cubic (FCC), body-centered cubic (BCC) or hexagonal close-packed (HCP) structure instead of complex intermetallic compounds [2,3]. These alloys display an excellent combination of properties such as high strength (>1.0 GPa) [4,5] and hardness (>5.8 GPa) [6], outstanding fracture toughness (>200 $MPa·m^{1/2}$) [7], good resistance against corrosion [8] and oxidation [9], and low wear rate [10].

In previous studies, FeCoNiCu(Cr)-based HEAs exhibit a high strength, high hardness and acceptable ductility, which is a promising alloy system in structural applications [11−13]. The addition of alloying elements into HEAs is known to further enhance their mechanical properties. For example, using the vacuum arc melting method, RAHUL et al [14] fabricated a series of $FeCoNiCuNb_x$ HEAs (x=0.5, 5, 7.5, 11.6 and 15 at.%), and it was found that the strength and hardness of those HEAs were simultaneously enhanced with increasing the concentration of Nb. RAHUL et al [15] also tailored the Sn content in $FeCoNiCuSn_x$ HEA and found that the micro-hardness of $FeCoNiCuSn_{0.5}$ alloy was improved due to the combination of solid solution strengthening

Corresponding author: He-guo ZHU, Tel: +86-13605182940, E-mail: zhg1200@njust.edu.cn
DOI: 10.1016/S1003-6326(23)66342-3

and microstructure refinement under undercooling condition. The hardness and wear resistance of $Al_xCrFeCoNiCu$ HEAs were greatly improved, due to the microstructure refinement and the formation of hard BCC phase [16]. In addition, by introducing Al into TiC/FeCoNiCu HEA composite, the tensile strength of the new alloy is significantly improved to 675 MPa along with the sacrifice of ductility [17].

Despite extensive efforts have devoted to improving the mechanical properties of FeCoNiCu(Cr)-based HEAs through the alloying approach, limited work has been done to explore the role of each individual non-metallic element (C or Si) on this system. Therefore, in order to reveal the relationship between the alloying elements and microstructure/mechanical properties of FeCoNiCu HEAs, we formulated two series of HEAs: $Fe_{2.5}CoNiCuSi_x$ (x=0.1, 0.15, 0.2, 0.25 and 0.3 in molar fraction) and $Fe_{2.5}CoNiCuC_x$ (x=0.15, 0.25, 0.35 and 0.4 in molar fraction). $Fe_{2.5}CoNiCu$ HEA was used as the reference metal, since its high hardness and high tensile strength identified in our previous work [18]. The influence of Si and C additions on the microstructure and mechanical properties of $Fe_{2.5}CoNiCu$ HEAs was studied and uncovered, in so doing offering new insight into the alloy design for enhanced mechanical properties.

2 Experimental

$Fe_{2.5}CoNiCu$ HEAs were prepared by the vacuum induction melting. The more detailed information of $Fe_{2.5}CoNiCu$ can be found in Ref. [18]. To reveal the influence of Si and C additions on the microstructure and mechanical properties of $Fe_{2.5}CoNiCu$ HEAs, we produced two series of HEAs: $Fe_{2.5}CoNiCuSi_x$ (x=0.1, 0.15, 0.2, 0.25 and 0.3 in molar fraction) and $Fe_{2.5}CoNiCuC_x$ (x=0.15, 0.25, 0.35 and 0.4 in molar ratio). The information of the raw materials is listed in Table 1. The raw materials were firstly placed in a ceramic crucible inside an induction melting furnace and heated to a molten state. The molten metal was poured into a copper mold with the dimension of d35 mm × 80 mm, and then cooled down to room temperature inside the furnace.

As-cast specimens with sizes of 10 mm × 10 mm × 6 mm (length × width × height) were used for microstructural characterization. An X-ray diffractometer (XRD, Bruker D8 Advance X) with a Cu K_α radiation was employed to analyze the phase constitution with a scanning range from 20° to 90° at a scanning speed 0.2 (°)/min. A field emission scanning electron microscope (FESEM, Quanta 250 FEG) equipped with an energy dispersive spectroscopy (EDS, Quanta 250 FEG) were conducted to observe the microstructure and the chemical compositions of the alloys at an acceleration voltage of 20 kV. The micro-hardness of specimens was measured by a hardness instrument (HVS−1000), and the applied load was 9.8 N and the duration time was 15 s. Five points were tested and the average micro-hardness was calculated. The density of specimens was analyzed by using the Archimedes method, and three measurements were taken. The tensile tests were conducted using specimens with a gauge geometry of 21.6 mm × 2.4 mm × 1.5 mm (length × width × height) at room temperature at a constant strain rate of 0.5 mm/min. The surface of the tensile specimens was ground to 2000 grit sand paper to remove surface asperities.

Table 1 Physical properties of raw materials used

Powder	Diameter/mm	Purity/%
Fe	2−3	99.99
Co	4−7	99.95
Ni	3−6	99.99
Cu	3−5	99.99
C	0.0005−0.003	99.85
Si	0.015−0.025	99.9

3 Result and discussion

3.1 Influence of Si on microstructural development of $Fe_{2.5}CoNiCuSi_x$ HEA

When the Si content is below 0.3, the $Fe_{2.5}CoNiCuSi_x$ alloys mainly contain a mix of FCC and BCC phases as shown in Fig. 1. With increasing Si content, the peak intensity of BCC phase gradually decreases, while the peak intensity of FCC phase steadily increases, which indicates that the fraction of FCC phase progressively increases in the alloy. As a result, the structure of the $Fe_{2.5}CoNiCuSi_x$ HEAs is gradually transformed from FCC/BCC dual phases to a single FCC phase when the Si content reaches 0.3. Meanwhile,

the main diffraction peak of the FCC phase slowly shifts to the left as the Si content increases, which is attributed to the lattice distortion caused by the Si addition [19].

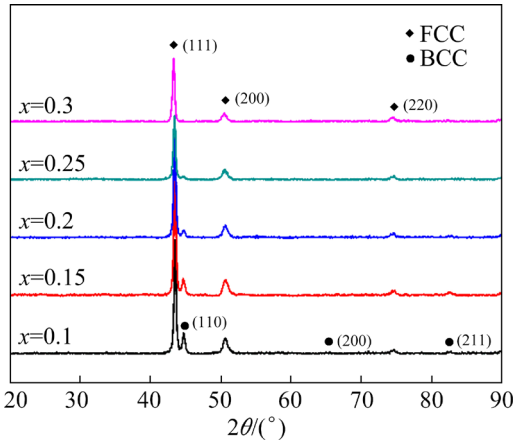

Fig. 1 XRD patterns of $Fe_{2.5}CoNiCuSi_x$ HEAs

Several parameters have been used to predict phase formation in HEAs, namely, mixing entropy (ΔS_{mix}), valence electron concentration (VEC) and atomic size difference (δ), which are expressed by Eqs. (1)−(4) [20,21].

$$VEC=\sum_{i=1}^{n} n_i VEC_i \quad (1)$$

$$\Delta S_{mix}=-R\sum_{i=1}^{n} n_i \ln n_i \quad (2)$$

$$\delta=100\times\sqrt{\sum_{i=1}^{n} n_i (1-r_i/\overline{r})^2} \quad (3)$$

$$\overline{r}=\sum_{i=1}^{n} n_i r_i \quad (4)$$

where n is the number of constituent elements, n_i is the molar fraction of the ith element, VEC_i is the VEC value of the ith element, R represents the molar gas constant (8.314 J/(mol·K), r_i is the atomic radius of the ith element, and $\overline{r}$ is the average atomic radius. As shown in Table 2, the VEC values of $Fe_{2.5}CoNiCuSi_x$ are calculated as 9.00, 8.96, 8.91, 8.87 and 8.83, respectively, which are all greater than 8, and mean that these alloys should be a single FCC phase [22]. However, the alloy is composed of FCC/BCC dual phases when the content of Si is below 0.3. The experimental results are thus in disagreement with the above prediction. Such abnormal phenomenon might be attributed to the high content of Fe in $Fe_{2.5}CoNiCu$ HEA [18]. Although Si addition is conducive to the formation of BCC phase [23], the increase of Si content in this alloy system also promotes the increase of mixing entropy of $Fe_{2.5}CoNiCuSi_x$ HEA, which results in the increase of the FCC phase fraction. The mixing entropy (ΔS_{mix}) of $Fe_{2.5}CoNiCu$ HEA is estimated to be 10.73 $J\cdot K^{-1}\cdot mol^{-1}$ [18]. With the increase of Si content, the ΔS_{mix} of $Fe_{2.5}CoNiCuSi_x$ HEA increases from 11.27 to 11.85 $J\cdot K^{-1}\cdot mol^{-1}$. The high-entropy effect of the alloy system is thus enhanced with the increase of mixing entropy. As a result, the formation of BCC phase is inhibited, which is consistent with the theoretical result of VEC (x=0.3).

Table 2 Parameters of $Fe_{2.5}CoNiCuSi_x$ HEAs

Alloy	ΔS_{mix}/ ($J\cdot K^{-1}\cdot mol^{-1}$)	VEC	$\overline{r}$ /Å	δ/%
$Si_{0.1}$	11.27	9.00	1.2496	1.43
$Si_{0.15}$	11.44	8.96	1.2488	1.54
$Si_{0.2}$	11.56	8.91	1.2479	1.64
$Si_{0.25}$	11.73	8.87	1.2474	1.74
$Si_{0.3}$	11.85	8.83	1.2466	1.83

The microstructures of $Fe_{2.5}CoNiCuSi_x$ HEAs are shown in Fig. 2, and the chemical compositions of the alloys are listed in Table 3. Figure 2 shows that dark spots present in the $Fe_{2.5}CoNiCuSi_x$ HEAs, which is consistent with an earlier study [18]. Figure 2(f) shows the EDS analysis of the Region *A* (dark spot) in Fig. 2(c), which suggests that the Fe content is high in dark regions. According to the previous work [18], the dark spots are Fe-rich precipitates with BCC structure. The dark spots disappeared when the Si content exceeded 0.25, and the volume fractions of BCC in $Fe_{2.5}CoNiCuSi_x$ HEAs were about 18.2%, 14.9%, 12.1%, 5.0% and 0.1%, respectively. The result is agreement with the XRD result (Fig. 1). The disappearance of the dark spots in the alloy might be related to the mixing entropy. The increase of mixing entropy apparently promotes the crystal structure of the alloy to gradually change into a single FCC structure, meaning that the Fe-rich precipitates are slowly absorbed by the FCC solid solution. Meanwhile, the actual composition of $Fe_{2.5}CoNiCuSi_x$ HEAs is closed to the nominal composition (Table 3), and the grain size of $Fe_{2.5}CoNiCuSi_x$ HEAs decreases from (24.61±3.86) to (13.02±6.18) μm with the

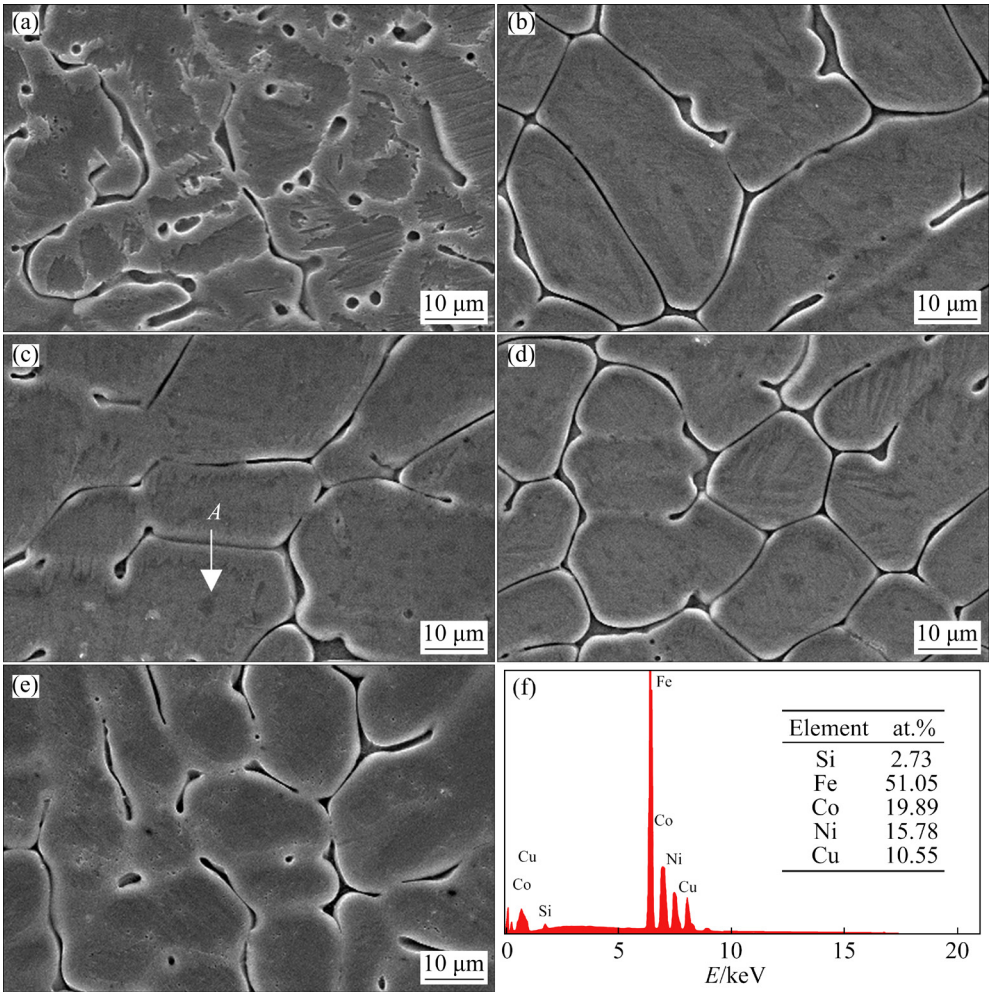

Fig. 2 Microstructures of $Fe_{2.5}CoNiCuSi_x$ HEAs with different contents of Si: (a) x=0.1; (b) x=0.15; (c) x=0.2; (d) x=0.25; (e) x=0.3; (f) EDS analysis of Region A

Table 3 Chemical compositions of $Fe_{2.5}CoNiCuSi_x$ HEAs by EDS analysis (at.%)

Alloy	Chemical composition	Fe	Co	Ni	Cu	Si
$Si_{0.1}$	Nominal	44.64	17.86	17.86	17.86	1.78
	Actual	49.84	19.77	17.22	11.58	1.59
$Si_{0.15}$	Nominal	44.25	17.70	17.70	17.70	2.65
	Actual	48.98	19.82	17.34	11.70	2.16
$Si_{0.2}$	Nominal	43.87	17.54	17.54	17.54	3.51
	Actual	49.84	19.38	16.56	11.01	3.21
$Si_{0.25}$	Nominal	43.49	17.39	17.39	17.39	4.34
	Actual	45.29	18.24	16.65	15.65	4.17
$Si_{0.3}$	Nominal	43.10	17.24	17.24	17.24	5.18
	Actual	44.58	18.12	17.90	14.04	5.36

increase of Si content. The grain refinement is supposedly relevant to the increase of lattice distortion. According to TAKEUCHI et al [23], the atomic radii of Fe, Co, Ni, Cu and Si are 1.24, 1.25, 1.25, 1.28 and 1.17 Å, respectively. The atomic size differences (δ) are respectively calculated as 1.43%, 1.54%, 1.65%, 1.74% and 1.83% in the alloys. Since the lattice distortion in the HEAs is positively correlated with atomic size difference [24], it can be inferred that the increase of lattice distortion leads to the grain refinement.

To further identify the elements distribution in $Fe_{2.5}CoNiCuSi_x$ HEAs, the EDS mapping results of $Fe_{2.5}CoNiCuSi_{0.2}$ HEA is shown in Fig. 3. It is shown that Cu element segregates in the inter-dendritic regions due to its positive enthalpy of mixing with Fe, Co and Ni elements; whereas Fe and Co elements have a higher content within the dendrite regions due to their high binary mixing enthalpy with Cu element. The Ni and Si elements are distributed homogeneously and no segregation phenomenon is observed. Therefore, the influence of Si element on the microstructural evolution of $Fe_{2.5}CoNiCuSi_x$ HEAs is less severe.

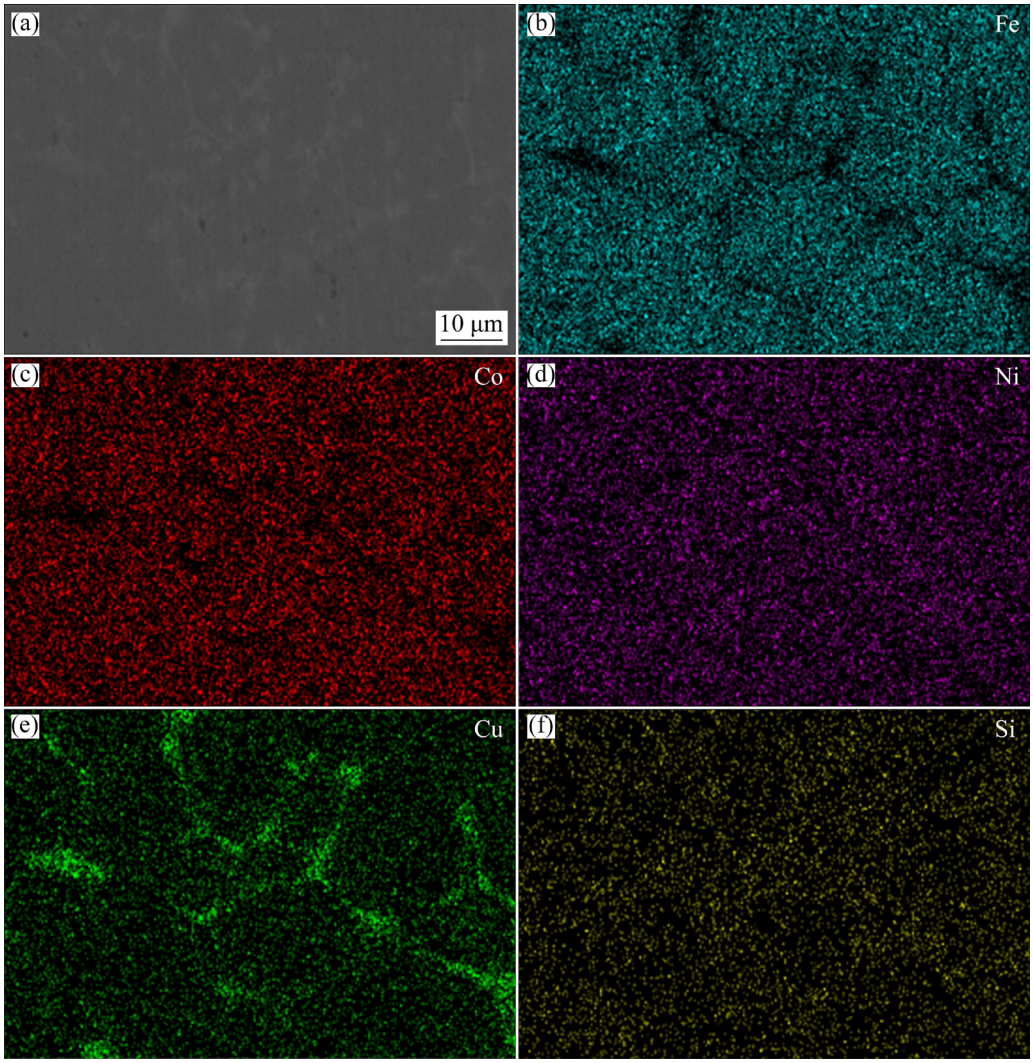

Fig. 3 Elemental mapping of $Fe_{2.5}CoNiCuSi_{0.2}$ HEA by EDS

3.2 Influence of C on microstructure of $Fe_{2.5}CoNiCuC_x$ HEAs

The microstructures of $Fe_{2.5}CoNiCuC_x$ HEAs are shown in Fig. 4. All alloys consist of a granular structure (*A*) and an intergranular structure (*B*). A very small number of bright particles appear discretely in the intergranular structure (Figs. 4(a) and (b)), and the chemical compositions of the particles are also listed in Table 4. The chemical composition of granular structure is close to nominal composition of alloys, but the particle is rich in C and Fe and depleted in Co, Ni and Cu. This implies that the particle is a typical C−Fe carbides. At x=0.35, the carbides are formed continually in the intergranular structure (Fig. 4(c)), which indicates that the C content exceeds the solubility limit of the $Fe_{2.5}CoNiCu$ HEA. Agglomerated carbides, some in large blocks, can be observed at x=0.4 (Fig. 4(d)), indicative of the C over-dose in the alloy.

Figure 5 shows the XRD patterns of $Fe_{2.5}CoNiCuC_x$ HEAs. All $Fe_{2.5}CoNiCuC_x$ HEAs have a single FCC structure. Since the VECs of C and Si are the same, their influence on the crystal structure of the alloys would be similar [25]. However, when a small amount of C was added (x<0.15), the alloy was transformed into a solution with single FCC phase. Such a significant change in the crystal structure is presumably associated with the interaction between the interstitial C atoms and Fe atoms [26].

Figure 6 shows the elemental mapping of $Fe_{2.5}CoNiCuC_{0.35}$ HEA. The results show that the content of Fe element in the carbide is slightly higher than that of other elements (Ni, Cu and Co). The segregation of Co element is not obvious, while

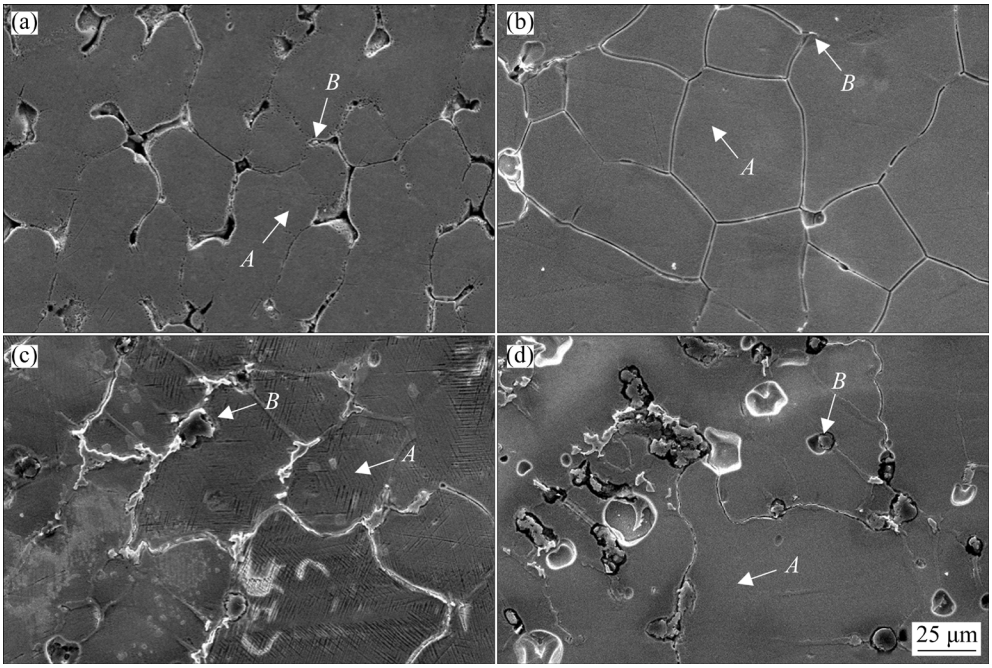

Fig. 4 Microstructures of $Fe_{2.5}CoNiCuC_x$ HEAs with different contents of C: (a) x=0.15; (b) x=0.25; (c) x=0.35; (d) x=0.4

Table 4 Chemical compositions of $Fe_{2.5}CoNiCuC_x$ HEAs by EDS analysis (at.%)

Alloy	Region	Fe	Co	Ni	Cu	C
	Nominal	44.25	17.70	17.70	17.70	2.65
$C_{0.15}$	*A*	41.37	21.64	20.43	13.35	3.21
	B	22.93	10.26	9.78	8.51	48.52
	Nominal	43.49	17.39	17.39	17.39	4.34
$C_{0.25}$	*A*	46.88	17.82	18.70	11.52	5.08
	B	23.71	8.82	6.86	4.91	55.70
	Nominal	42.74	17.09	17.09	17.09	17.09
$C_{0.35}$	*A*	43.91	17.54	16.66	15.66	6.23
	B	25.01	10.18	7.59	4.49	52.73
	Nominal	42.37	16.95	16.95	16.95	6.78
$C_{0.4}$	*A*	48.59	16.46	16.17	11.56	7.22
	B	19.49	9.41	8.26	6.01	56.83

the content of Ni and Cu elements is lower than that in the alloy, which might be attributed to the difference in the binary mixing enthalpy of C element with Fe, Co, Ni and Cu elements. According to TAKEUCHI et al [23], the binary mixing enthalpies of C with Fe, Co, Ni and Cu are −50, −42, −39 and −33 kJ/mol. Since the binary mixing enthalpy of Fe and C is the lowest, the C atoms would bond easily with Fe atoms. The high

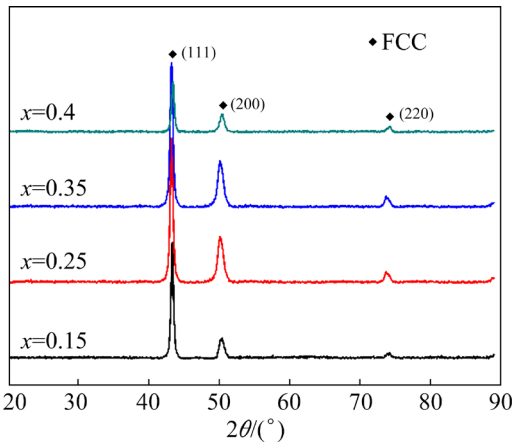

Fig. 5 XRD patterns of $Fe_{2.5}CoNiCuC_x$ HEAs

chemical affinity between C and Fe atoms would enhance the stability of the FCC structure and as such reduce Fe-rich BCC phase in the alloy, which might be responsible for the microstructure transformation of $Fe_{2.5}CoNiCu$ HEA.

Based on the above analysis, the Si addition not only promotes the dissolution of BCC phase into the FCC phase, but also increases the alloy lattice distortion and reduces the grain size (Figs. 1 and 2). The addition of C facilitates the formation of carbides in the intergranular structures when the C content is high. Additionally, the C element can significantly reduce the fraction of BCC phase and convert the alloy into a single FCC structure. Both

the Si and C elements can stimulate the transformation of BCC/FCC dual-phases structure into a single FCC structure, but the microstructural evolution appears to be more strongly influenced by the C addition.

3.3 Influence of Si on mechanical properties of $Fe_{2.5}CoNiCuSi_x$ HEAs

Figure 7(a) shows the engineering stress−strain curves of $Fe_{2.5}CoNiCuSi_x$ HEAs at room temperature. The fracture elongation of $Fe_{2.5}CoNiCuSi_x$ HEAs steadily decreases from 8.0% to 4.1% with addition of Si element, which indicates that the $Fe_{2.5}CoNiCuSi_x$ HEAs become brittle. Although the plasticity of the alloy is reduced, the strength of the alloy increases when a small amount of Si is added. The ultimate tensile strength (UTS) of $Fe_{2.5}CoNiCuSi_{0.1}$ increases by

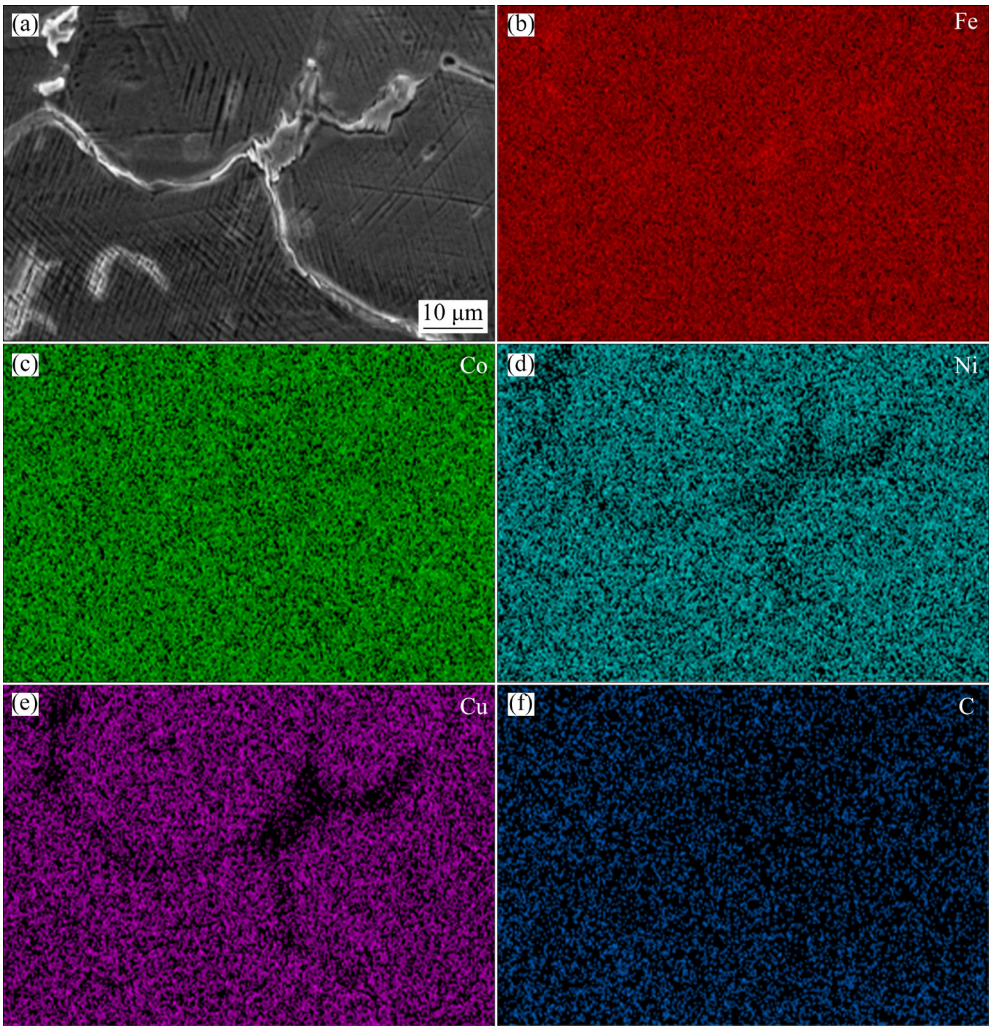

Fig. 6 Elemental mapping for $Fe_{2.5}CoNiCuC_{0.35}$ HEA by EDS

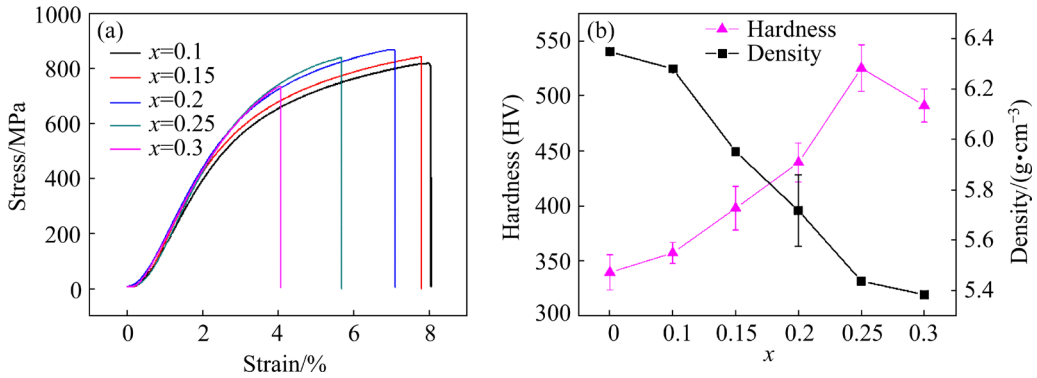

Fig. 7 Engineering stress−strain (a) and hardness and density (b) curves of $Fe_{2.5}CoNiCuSi_x$ HEAs

about 180 MPa compared with $Fe_{2.5}CoNiCu$ HEA (639 MPa) [18]. The UTS of $Fe_{2.5}CoNiCuSi_{0.2}$ reaches a maximum value of 868 MPa, which is higher than the SiC/$Fe_{2.5}CoNiCu$ composite (787 MPa) [27]. After the C content exceeds 0.2 at.%, both the strength and plasticity of $Fe_{2.5}CoNiCuSi_x$ decrease simultaneously. The hardness and density of $Fe_{2.5}CoNiCuSi_x$ HEAs are shown in Fig. 7(b). The hardness of $Fe_{2.5}CoNiCuSi_x$ HEAs monotonically increases at $x \leq 0.25$ and then decreases to HV 491.2 at x=0.3. The density of $Fe_{2.5}CoNiCuSi_x$ HEAs is gradually decreases from 6.35 to 5.38 g/cm^3 with the increase of Si content. As shown in Fig. 1, owe to the addition of alloying elements with large atomic radii, the lattice distortion in the FCC matrix is enhanced, which increases the resistance to dislocation movement, thereby boosting the strength and hardness [20]. Moreover, the size of grain is gradually refined with addition of Si as shown in Fig. 2, thus both the hardness and strength are improved due to the grain refinement effect. Therefore, the increment in strength and hardness of the $Fe_{2.5}CoNiCuSi_x$ HEAs is closely related to the addition of the Si element, which plays a role in the grain refinement and solid solution strengthening (Figs. 1 and 2).

Figure 8 shows the tensile fracture surface morphologies of $Fe_{2.5}CoNiCuSi_x$ HEAs. When a small amount of Si element was added (x=0.1 and 0.15), many small dimples can be seen on the fracture surface, while a few smooth fracture surfaces can also be observed. The number of dimples decreases gradually as the content of Si (x=0.2 and 0.25) increases. When x=0.3, the number of dimples decreases appreciably and some dendrites can be seen on the fracture surface, indicating that the addition of Si renders the material brittle. Consequently, the fracture mechanism of $Fe_{2.5}CoNiCuSi_x$ HEAs is translated from quasi-cleavage fracture to brittle fracture with the increase of Si content.

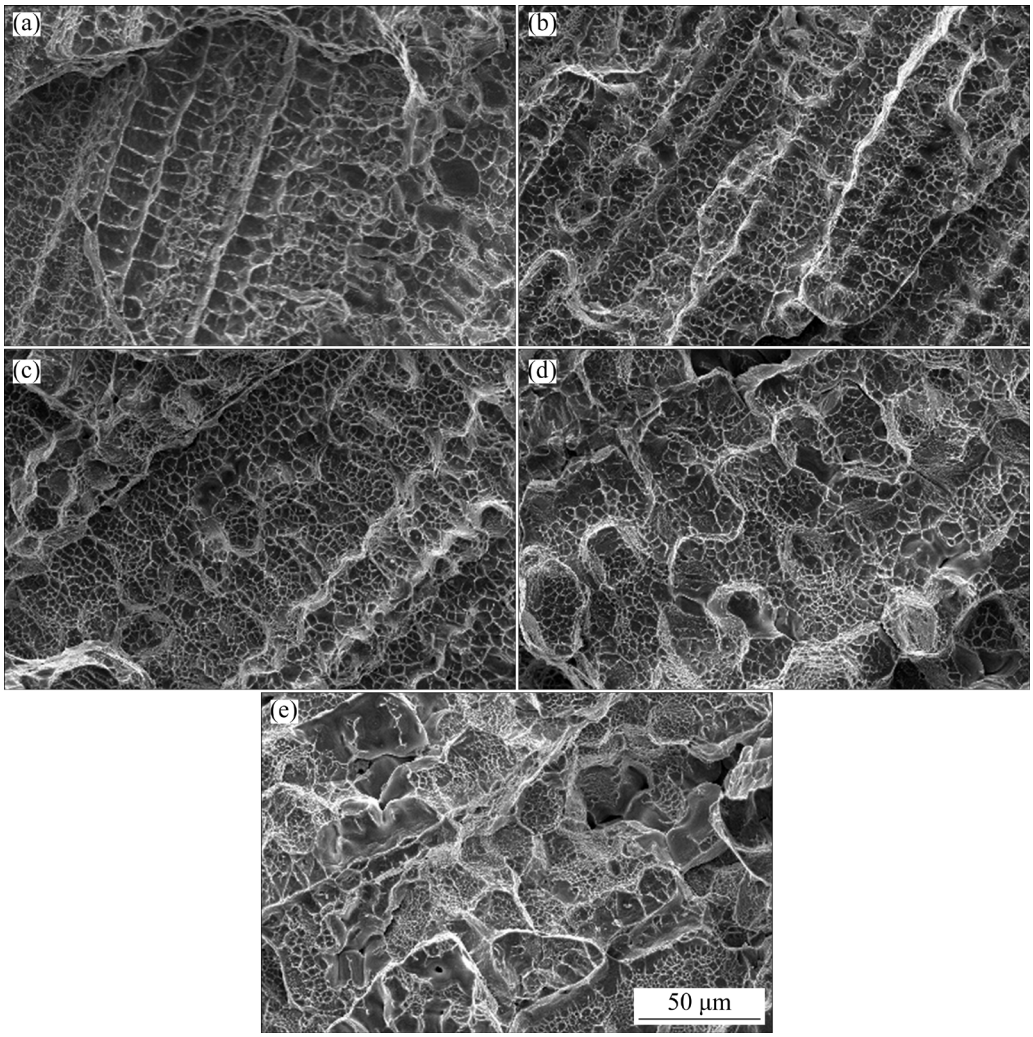

Fig. 8 Tensile fractured surface morphologies of $Fe_{2.5}CoNiCuSi_x$ HEAs: (a) x=0.1; (b) x=0.15; (c) x=0.2; (d) x=0.25; (e) x=0.3

3.4 Influence of C on mechanical properties of $Fe_{2.5}CoNiCuC_x$ HEAs

The engineering stress−strain curves of $Fe_{2.5}CoNiCuC_x$ HEAs are shown in Fig. 9(a). The C addition has a marked influence on the ductility of $Fe_{2.5}CoNiCuC_x$ HEAs. The fracture elongation of $Fe_{2.5}CoNiCuC_{0.15}$ increases to 15.6% with sacrificing a little strength as compared to $Fe_{2.5}CoNiCu$ HEA. The decreased strength could be related to the single FCC structure of $Fe_{2.5}CoNiCuC_{0.15}$ (Fig. 5). Both the strength and ductility of $Fe_{2.5}CoNiCuC_{0.25}$ simultaneously increase with further addition of C element, which are about 626 MPa and 21.7%, respectively. The fracture elongation and UTS of $Fe_{2.5}CoNiCuC_{0.35}$ are increased to 43.4% and 729 MPa, respectively. When the content of C element is 0.4 at.%, the UTS is slightly improved but the fracture elongation begins to decrease, which is indicative of C over-dose. Generally speaking, the degree of lattice distortion caused by interstitial atoms is severer than that induced by substitutional atoms [28]. The interstitial atoms thus have a great effect on dislocation mobility. Additionally they may affect the phase stability via altering the stacking fault energy of the alloy, which in turn impact the properties of the alloy [29]. WANG et al [30,31] observed that the strength and ductility of $Fe_{40.4}Ni_{11.3}Mn_{34.8}$- $Al_{7.5}Cr_6$ increased simultaneously with the addition of element C, which is attributed to that the interstitial C atoms in the alloy not only reduced the stacking fault energy, but also increased the frictional stress of lattice. CHEN et al [32] also found that interstitial C atoms can play a twin toughening effect in high entropy alloys. Therefore, the addition of C element is beneficial to improving the ductility and tensile strength of $Fe_{2.5}CoNiCuC_x$ HEAs. It also reveals that for $Fe_{2.5}CoNiCu$ HEA the better mechanical properties can be obtained by adding C rather than Si element. The hardness and density of $Fe_{2.5}CoNiCuC_x$ HEAs with different C contents are given in Fig. 9(b). With increase of C content, the hardness is increased from HV 339.6 to HV 440.4, while the density is increased initially and then decreased monotonically. The increment in hardness is attributed to the formation of carbides in alloy matrix to hinder the dislocation movement [33].

The fracture surface of $Fe_{2.5}CoNiCuC_x$ HEAs is plotted in Fig. 10. As shown in Fig. 10(a), a large number of small dimples (red circle) can be seen on the fracture surface of $Fe_{2.5}CoNiCuC_{0.15}$ HEA. Figure 10(b) shows the fracture morphology of $Fe_{2.5}CoNiCuC_{0.25}$ HEA, which is different from that of $Fe_{2.5}CoNiCuC_{0.15}$ HEA. The small dimples were no longer observed in the fracture but were replaced by large and deep dimples, suggesting that the ductility of the alloy is improved. The fracture morphology of $Fe_{2.5}CoNiCuC_{0.35}$ HEA is also different from that of $Fe_{2.5}CoNiCuC_{0.25}$ HEA (Fig. 10(c)). An increasing number of large dimples can be observed on the fracture surface, with some carbides lodged in the dimples as shown by the yellow circle. The dimples are deeper, indicating that the ductility of the alloy is further improved. The presence of these carbides in the alloy not only enhanced the ductility, but also improved the strength of the alloy [33]. The number of dimples on the fracture surface of $Fe_{2.5}CoNiCuC_{0.4}$ HEA significantly decreases and the depth also becomes shallower in Fig. 10(d). Moreover, a large number of carbides can be seen in the alloy (yellow circle), which compromises the ductility of the alloy.

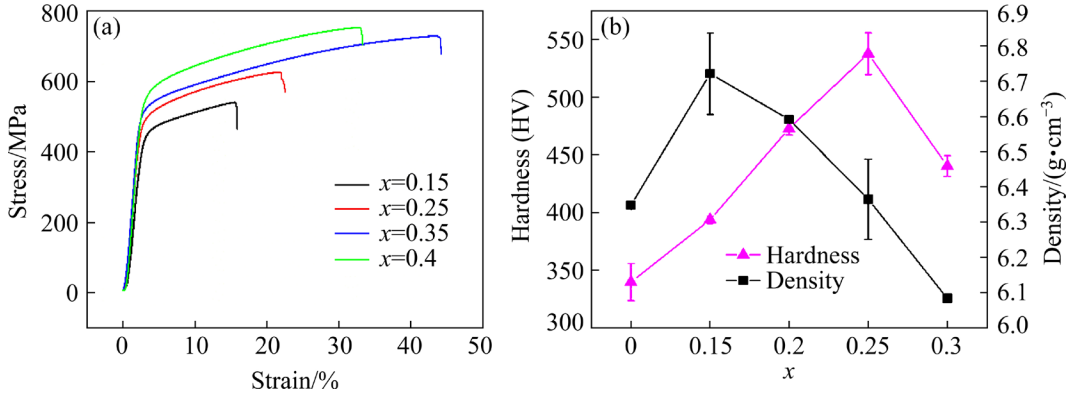

Fig. 9 Engineering stress−strain (a) and hardness and density (b) curves of $Fe_{2.5}CoNiCuC_x$ HEAs

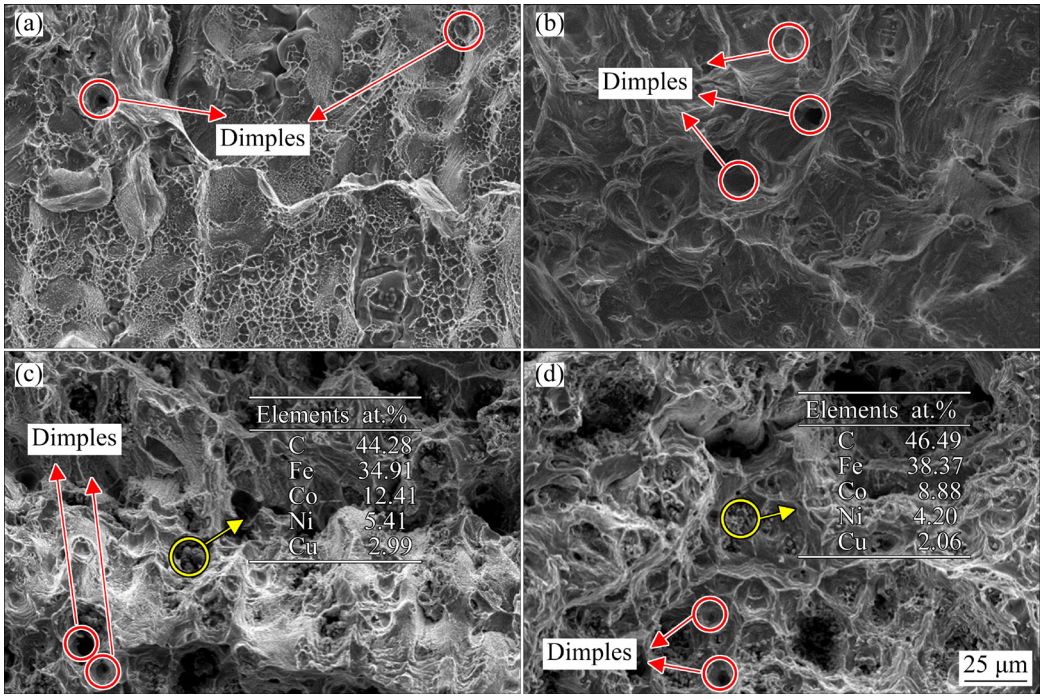

Fig. 10 Tensile fractured surface morphologies of $Fe_{2.5}CoNiCuC_x$ HEAs: (a) x=0.15; (b) x=0.25; (c) x=0.35; (d) x=0.4

4 Conclusions

(1) Both the Si and C elements are found to inhibit the formation of BCC phase in $Fe_{2.5}CoNiCu$ alloys. The microstructure evolution of the alloy is severely affected by varying the C element.

(2) The Si addition can improve the strength of $Fe_{2.5}CoNiCu$ alloy through the grain refinement effect and solid solution strengthening.

(3) The C addition can effectively inhibit the emergence of BCC phase and promote the formation of carbides, thereby improving the ductility and strength of $Fe_{2.5}CoNiCu$ HEAs simultaneously.

Acknowledgments

This work was financially supported by the National Natural Science Foundation of China (No. 51571118).

References

[1] YEH Jien-wei, CHEN Swe-kai, LIN Su-jien, GAN Jon-yiew, CHIN Tsung-shune, SHUN Tao-tsung, TASU Chun-huei, CHANG Shou-yi. Nanostructured high-entropy alloys with multiple principal elements novel alloy design concepts and outcomes [J]. Advanced Engineering Materials, 2004, 6(5): 299−303.

[2] GEORGE E P, RAABE D, RITCHIE R O. High-entropy alloys [J]. Nature Reviews Materials, 2019, 4(8): 515−534.

[3] ZHANG Yong, ZUO Ting-ting, TANG Zhi, GAO M C, DAHMEN K A, LIAW P K. LU Zhao-ping. Microstructures and properties of high-entropy alloys [J]. Progress in Materials Science, 2014, 61: 1−93.

[4] TONG Y, CHEN D, HAN B, WANG J, FENG R, YANG T, ZHAO C, ZHAO Y L, GUO W, SHIMIZU Y, LIU C T, LIAW P K, INOUE K, NAGAI, Y, HU A, KAI J J. Outstanding tensile properties of a precipitation-strengthened FeCoNiCrTi0.2 high-entropy alloy at room and cryogenic temperatures [J]. Acta Materialia, 2019, 165: 228−240.

[5] DU Hui, CAI Jia-hong, WANG Ya-song, YAO Jun-qing, CHEN Qiang, CUI Yu, LIU Xin-wang. Effect of partial recrystallization on microstructure and tensile properties of NiFeCoCrMn high-entropy alloy [J]. Transactions of Nonferrous Metals Society of China, 2022, 32(3): 947−956.

[6] SENKOV O N, SENKOVA S V, WOODWARD C. Effect of aluminum on the microstructure and properties of two refractory high-entropy alloys [J]. Acta Materialia, 2014, 68: 214−228.

[7] GLUDOVATZ B, HOHENWARTER A, CATOOR D, CHANG E H, GEORGE E P, RITCHIE R O. A fracture-resistant high-entropy alloy for cryogenic applications [J]. Science, 2014, 345(6201): 1153−1158.

[8] ZHOU En-ze, QIAO Dong-xu, YANG Yi, XU Da-ke, LU Yi-ping, WANG Jian-jun, SMITH J A, LI Hua-bing, ZHAO Hong-liang, LIAW P K, WANG Fu-hui. A novel Cu-bearing high-entropy alloy with significant antibacterial behavior against corrosive marine biofilms [J]. Journal of Materials Science & Technology, 2020, 46: 201−210.

[9] CAO Yuan-kui, LIU Yong, LIU Bin, ZHANG Wei-dong, WANG Jia-wen, DU Meng. Effects of Al and Mo on high

temperature oxidation behavior of refractory high entropy alloys [J]. Transactions of Nonferrous Metals Society of China, 2019, 29(7): 1476−1483.

[10] XIAO Wei-Cheng, LI Kun, HAN Liu-liu, LIU Yong. Self-lubricating behavior of Fe22Co26Cr20Ni22Ta10 high-entropy alloy matrix composites [J]. Transactions of Nonferrous Metals Society of China, 2021, 31(3): 744−752.

[11] HE J Y, LIU W H, WANG H, WU Y, LIU X J, NIEH T G, LU Z P. Effects of Al addition on structural evolution and tensile properties of the FeCoNiCrMn high-entropy alloy system [J]. Acta Materialia, 2014, 62: 105−113.

[12] XIAO Jin-kun, WU Yu-qing, CHEN Juan, ZHANG Chao. Microstructure and tribological properties of plasma sprayed FeCoNiCrSiAl$_x$ high entropy alloy coatings [J]. Wear, 2020, 448/449: 203209.

[13] ZHANG Yi-tan, LIU Mao-wen, SUN Jing-yong, LI Guo-dong, ZHENG Rui-xiao, XIAO Wen-long, MA Chao-li. Excellent thermal stability and mechanical properties of bulk nanostructured FeCoNiCu high entropy alloy [J]. Materials Science and Engineering A, 2022, 835: 142670.

[14] RAHUL M R, SAMAL S, PHANIKUMAR G. Effect of niobium addition in FeCoNiCuNbx high-entropy alloys [J]. Journal of Materials Research, 2019, 34(5): 700−708.

[15] RAHUL M R, PHANIKUMAR G. Growth kinetics, microhardness and microstructure evolution of undercooled FeCoNiCuSn high entropy alloy [J]. Materials Science and Engineering A, 2020, 777: 139022.

[16] JI Xiu-lin, ALAVI S H, HARIMKAR S P, ZHANG Ying-tao. Sliding wear of spark plasma sintered CrFeCoNiCu high-entropy alloy coatings: Effect of aluminum addition [J]. Journal of Materials Engineering and Performance, 2018, 27(11): 5815−5822.

[17] SUN Xiao-dong, ZHU He-guo, LI Jian-liang, HUANG Jie-wen, XIE Zong-han. Influence of aluminum content on the microstructure and properties of the in-situ TiC reinforced Al$_x$FeCoNiCu high entropy alloy matrix composites [J]. Materials Science and Engineering A, 2019, 743: 540−545.

[18] QIU Huan, ZHU He-guo, ZHANG Ji-feng, XIE Zong-han. Effect of Fe content upon the microstructures and mechanical properties of Fe$_x$CoNiCu high entropy alloys [J]. Materials Science and Engineering A, 2020, 769: 138514.

[19] CHENG Peng, ZHAO Yu-hong, XU Xiao-tao, WANG Shuai, SUN Yuan-yang, HOU Hua. Microstructural evolution and mechanical properties of Al0.3CoCrFeNiSi$_x$ high-entropy alloys containing coherent nanometer-scaled precipitates [J]. Materials Science and Engineering A, 2020, 772: 138681.

[20] LIU Xiao-tao, LEI Wen-bin, MA Li-juan, LIU Jing, LIU Jin-ling, CUI Jian-zhong. On the microstructures, phase assemblages and properties of Al0.5CoCrCuFeNiSi$_x$ high-entropy alloys [J]. Journal of Alloys and Compounds, 2015, 630: 151−157.

[21] ZHU Cheng-Yan, WU Hao, ZHU He-guo, LI Xiang-dong, TU Chun-lei, XIE Zong-han. Mechanical properties and fracture mechanism of as-cast MnFeCoCuNi high-entropy alloys [J]. Transactions of Nonferrous Metals Society of China, 2021, 31(1): 222−231.

[22] JIN Xi, ZHOU Yang, ZHANG Lu, DU Xing-yu, LI Bang-sheng. A new pseudo binary strategy to design eutectic high entropy alloys using mixing enthalpy and valence electron concentration [J]. Materials & Design, 2018, 143: 49−55.

[23] TAKEUCHI A, INOUE A. Classification of bulk metallic glasses by atomic size difference, heat of mixing and period of constituent elements and its application to characterization of the main alloying element [J]. Materials Transactions, 2005, 46(12): 2817−2829.

[24] WANG Zhi-jun, QIU Wei-feng, YANG Yong, LIU C T. Atomic-size and lattice-distortion effects in newly developed high-entropy alloys with multiple principal elements [J]. Intermetallics, 2015, 64: 63−69.

[25] GUO Sheng, LIU C T. Phase stability in high entropy alloys: Formation of solid-solution phase or amorphous phase [J]. Progress in Natural Science: Materials International, 2011, 21(6): 433−446.

[26] KHAPLE S, SATYANARAYANA D V V, SATYA PRASAD V V, GOLLA B R. Evolution of microstructure with increasing carbon content and its effect on mechanical properties of disordered iron–aluminium alloy [J]. Bulletin of Materials Science, 2019, 42(5): 234.

[27] WU Jian, QIU Huan, ZHU He-guo, XIE Zong-han, CHEN Jia-lin. Microstructure and mechanical behaviors of in-situ SiC particle reinforced Fe2.5CoNiCu high-entropy alloy composites [J]. Materials Letters, 2022, 311: 131495.

[28] OHNUMA T, SONEDA N, IWASAWA M. First-principles calculations of vacancy–solute element interactions in body-centered cubic iron [J]. Acta Materialia, 2009, 57(20): 5947−5955.

[29] LI Zhi-ming. Interstitial equiatomic CoCrFeMnNi high-entropy alloys: Carbon content, microstructure, and compositional homogeneity effects on deformation behavior [J]. Acta Materialia, 2019, 164: 400−412.

[30] WANG Zhang-wei, BAKER I, CAI Zhong-huo, CHEN Si, POPLAWSKY J D, GUO Wei. The effect of interstitial carbon on the mechanical properties and dislocation substructure evolution in Fe40.4Ni11.3Mn34.8Al7.5Cr6 high entropy alloys [J]. Acta Materialia, 2016, 120: 228−239.

[31] WANG Zhang-wei, BAKER I. Interstitial strengthening of a f.c.c. FeNiMnAlCr high entropy alloy [J]. Materials Letters, 2016, 180: 153−156.

[32] CHEN Jian, YAO Zhi-hao, WANG Xiao-bo, LU Yu-kun, WANG Xian-hui, LIU Yong, FAN Xin-hui. Effect of C content on microstructure and tensile properties of as-cast CoCrFeMnNi high entropy alloy [J]. Materials Chemistry and Physics, 2018, 210: 136−145.

[33] HUANG Tian-dang, JIANG Li, ZHANG Chang-liang, JIANG Hui, LU Yi-ping, LI Ting-ju. Effect of carbon addition on the microstructure and mechanical properties of CoCrFeNi high entropy alloy [J]. Science China Technological Sciences, 2018, 61(1): 117−123.

Si 和 C 的添加对 $Fe_{2.5}CoNiCu$ 高熵合金显微组织和力学性能的影响

吴 健[1]，邱 欢[1]，朱和国[1]，谢宗翰[2]，成家林[3]

1. 南京理工大学 材料科学与工程学院，南京 210094；
2. School of Mechanical Engineering, University of Adelaide, SA 5005, Australia；
3. 南京工程学院 材料科学与工程学院，南京 210094

摘 要：为了评估非金属元素(Si 和 C)对 $Fe_{2.5}CoNiCu$ 高熵合金显微组织演变和力学性能的影响，采用真空感应熔炼法制备 $Fe_{2.5}CoNiCuSi_x$ (x=0.1~0.3，摩尔分数)和 $Fe_{2.5}CoNiCuC_x$ (x=0.15~0.4，摩尔分数)两种系列高熵合金。结果表 明，C 和 Si 的加入显著促进 BCC/FCC 双相向单一 FCC 结构的转变，且添加 C 对 BCC/FCC 组织演变的影响更明显。$Fe_{2.5}CoNiCuSi_{0.2}$ 高熵合金具有较高的硬度(HV 439.5)和抗拉强度(868 MPa)，这与固溶强化和晶粒细化作用有关。随着 C 含量的增加，$Fe_{2.5}CoNiCuC_x$ 高熵合金的硬度和强度均增加，这是碳化物的形成和固溶强化所致。这表明在高熵合金中添加非金属元素(C 或 Si)是提高合金强度和硬度的可行途径。

关键词：高熵合金；显微组织演变；力学性能；非金属元素添加；断裂机制

(Edited by Xiang-qun LI)